Lab report
E213 Analysis of Z^0 Decay

Chenhuan Wang and Harilal Bhattarai

October 27, 2020

This is abstract.

1. Introduction

The Standard Model is essentially a gauge theory with $\mathbf{SU}(3)_C \times \mathbf{SU}(2) \times \mathbf{U}(1)_Y$. The $\mathbf{SU}(2) \times \mathbf{U}(1)$ contains four gauge fields and after symmetry breaking, because of vacuum expectation value of Higgs field, they into $W^{\pm}$, Z^0 and γ fields. Unlike γ which is massless and described by QED, Z^0 is massless and couple differently to different chiralities [1].

In this experiment we want to determine several properties of Z^0 boson, its mass, decay width and couplings. As a byproduct the analysis, we are also able to verify lepton universality and find out number of neutrino generations.

Here we briefly discuss theory and pre-lab problems in first two chapters. Then procedures and analysis of data by events display and statistical analysis in next two chapters will be illustrated.

2. Background

We will not try to derive the whole electroweak theory again. Here only some important, relevant equations and experimental setups are presented.

Decay width The partial decay width of Z^0 decay into fermion f is [2]

$$\Gamma_f = \frac{\sqrt{2} N_c^f}{12\pi} G_F M_Z^3 \left((g_V^f)^2 + (g_A^f)^2 \right) \tag{1}$$

with

$$g_V^f = I_3^f - 2Q_f \sin^2 \theta_W$$
$$g_A^f = I_3^f$$

One needs to be aware that Γ_f contains contribution from both chiralities, and I_3 here refers to only the weak isospin of left-handed fermions (by definition right handed fermions have no weak isospin).

Partial cross section of $Z^0 \to f\bar{f}$ is given by [2]

$$\sigma_f(s) = \frac{12\pi}{M_Z^2} \frac{s\Gamma_e\Gamma_f}{(s - M_Z^2)^2 + (s^2\Gamma_Z^2/M_Z^2)} \tag{2}$$

and exactly at peak of resonance

$$\sigma_{f,\text{peak}} = \frac{12\pi}{M_Z^2} \frac{\Gamma_e\Gamma_f}{\Gamma_Z^2} \tag{3}$$

Angular distribution In $ee \to ee$ scattering, two relevant channels have different angular dependences. For s-channel [2],

$$\left(\frac{\mathrm{d}\sigma}{\mathrm{d}\Omega}\right)_s \sim (1 + \cos^2\Theta) \tag{4}$$

For t-channel,

$$\left(\frac{\mathrm{d}\sigma}{\mathrm{d}\Omega}\right)_t \sim (1 - \cos^2\Theta)^{-2} \tag{5}$$

Forward-Backward Asymmetry is defined as

$$A_{FB} = \frac{N_+ - N_-}{N_+ + N_-} \tag{6}$$

where $N_{+,-}$ denotes number of events in forward or backward direction.

Near Z^0 resonance can be approximated by [2]

$$
\begin{aligned}
A_{\text{FB}}^f &\approx \frac{-3}{2} \frac{a_e a_f Q_f \,\text{Re}(\chi)}{(v_e^2 + a_e^2)(v_f^2 + a_f^2)} \\
&= \frac{-3}{2} \frac{a_e a_f Q_f}{(v_e^2 + a_e^2)(v_f^2 + a_f^2)} \frac{s(s - M_Z^2)}{(s - M_Z^2)^2 + (s\Gamma_Z/M_Z)^2}
\end{aligned}
\tag{7}
$$

Exactly at resonance peak, we have

$$A_{\text{FB}}^{l,\text{peal}} \approx 3\left(\frac{v_l}{a_l}\right)^2 = 3\left(\frac{I_3^l - 2Q_l \sin^2\theta_W}{I_3^l}\right)^2 \tag{8}$$

The OPAL-Detector We have used data in this experiment from OPAL detector. OPAL was one of the four detector devices at LEP at the CERN [2]. The collision point is surrounded by an central detector along with a vertex chamber, jet- and Z-chambers. The main function of all these chambers is to track the charged particles. The whole device is situated within an autoclave contains a mixture of argon, methane and isobutane at a pressure of 4 bar [2].

The central detector is surrounded by two calorimeters: electromagnetic calorimeter (ECAL) and hadronic calorimeter (HCAL). ECAL consists of lead glass blocks and surrounding jet chamber. The cathod pads are arranged behind these blocks. The energy and position of the electromagnetic showers are determined by th signal from cathode pads. The electron-positron particle showers deposited their energy in ECAL. Hadrons deposited their some part of energy in ECAL and rest of the part in HCAL [2].

Whole set-up is surrounded by the muon chamber. A forward detector (FCAL) is arranged close to the beam pipe consist of a sandwich of lead glass. It is used to measured the luminosity [2].
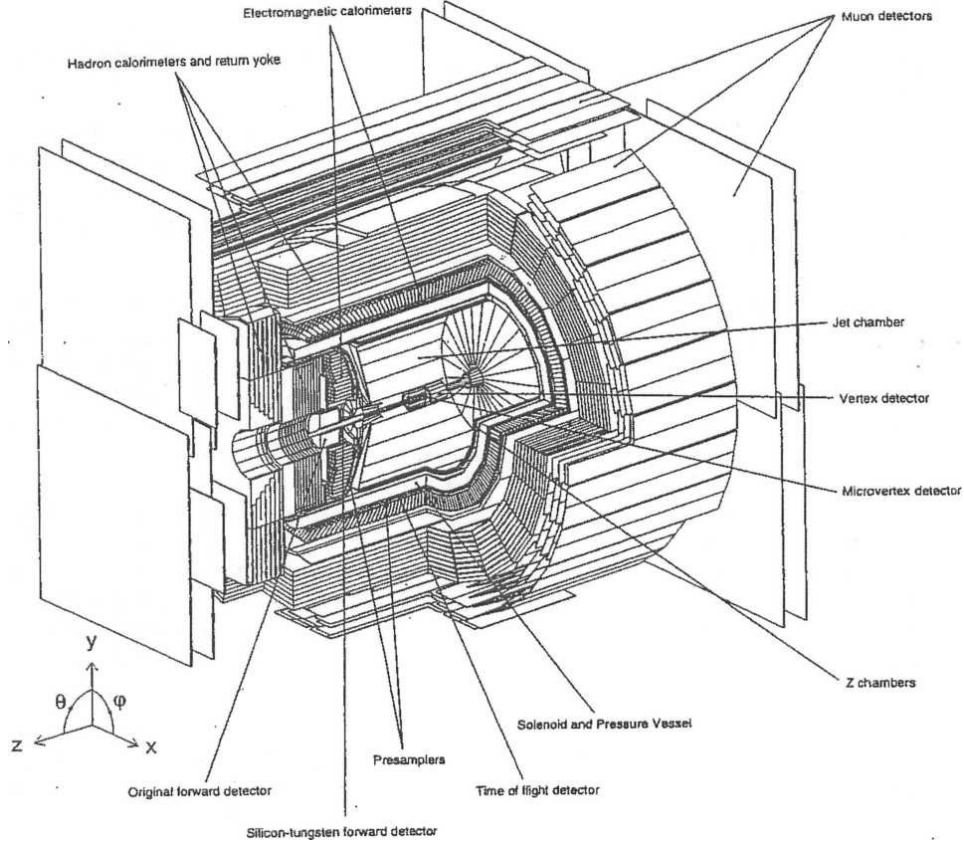

Figure 1: The OPAL detector [2].

3. Pre-lab tasks

Using equation 1, one finds

$$\Gamma_e = \Gamma_\mu = \Gamma_\tau = 83.40\,\text{MeV} \tag{9}$$

The decay widths to leptons of three generations are the same because of lepton universality (neglecting mass). With the same equation, decay widths to quarks are

$$\Gamma_u = \Gamma_c \qquad = 285.34\,\text{MeV}$$
$$\Gamma_d = \Gamma_s = \Gamma_b = 367.79\,\text{MeV}$$

It is significantly larger, mainly because of more degrees of freedom (color) than leptons. Decays to neutrinos are invisible for detector in LEP, but still they have the width of

$$\Gamma_\nu = 165.84\,\text{MeV} \tag{10}$$

Hadronic part in total

$$\Gamma_\text{h} = \sum_{\forall q \neq t} \Gamma_q = 1674.06\,\text{MeV} \tag{11}$$

3

Charged decay

$$\Gamma_{\text{charged}} = 3\Gamma_e = 250.17\,\text{MeV} \tag{12}$$

Invisible decay

$$\Gamma_{\text{inv}} = 3\Gamma_\nu = 497.52\,\text{MeV} \tag{13}$$

In total (except unknown decays)

$$\Gamma_{\text{total}} = 3\Gamma_e + \Gamma_h + 3\Gamma_\nu = 2421.75\,\text{MeV} \tag{14}$$

These values are listed in table 1.

decay type	partial width[MeV]	partial cross section[10^{-11}MeV^{-2}]
hadronic	1674.06	10.79
charged	250.17	1.61
invisible	497.52	3.21
total	2421.75	15.61

Table 1: Decays widths and partial cross sections

Assume that there is another generation of light fermions, the total width of Z^0 would be

$$\Gamma'_{\text{total}} = \Gamma_{\text{total}} + \Gamma_e + \Gamma_\nu + \Gamma_u + \Gamma_d = 3324.11\,\text{MeV} \tag{15}$$

It would be a change of 37% percent!

The differential cross section $\frac{\mathrm{d}\sigma}{\mathrm{d}\Omega}$ has different angular dependencies for s- and t-channels, see equations 4 and 5. Simply plotting without the proportional constant in front shows where s- or t-channels dominates the process, see figure. 2. At small angles, t-channel dominates, whereas at large angles, s-channel dominates.

One can try to calculate the forward-backward asymmetry in $Z^0 \to \mu\mu$ channel with equation 7. These are in table 2

$\sqrt{s}[\text{GeV}]$ /$\sin^2(\theta_W)$	0.21	0.23	0.25
89.225	-0.0379	-0.0420	-0.0451
91.225	-0.0386	-0.0428	-0.0459
93.225	-0.0394	-0.0436	-0.0468

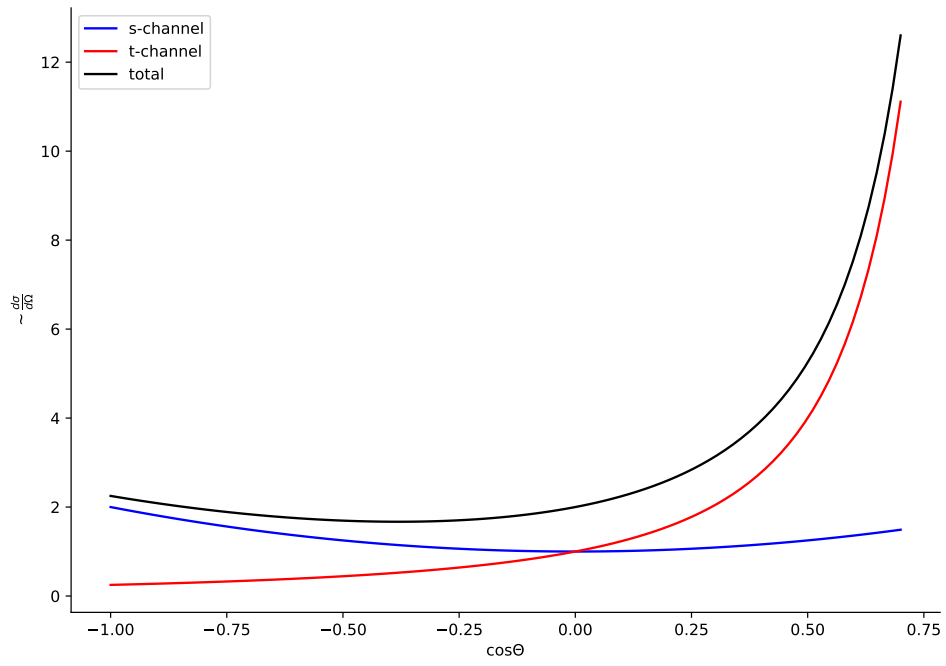Table 2: Forward-backward asymmetry in $Z^0 \to \mu\mu$ channel

Figure 2: Angular dependencies of two channels.

4. Event display

In this part, we focused on learning how to distinguish different channel by event display and four different variables. All channels have 20 events.

4.1. Identification of the particle at the OPAL detector

To identify the particles, firstly, we divide all particle in charged and uncharged on the basis of visible trajectory in proportional chamber. The charged hadrons and electrons are separated on the basis of their form and beginning of the shower. The electromagnetic showers caused by an electron have small lateral spread and completely situated with in the electromagnetic calorimeter (ECAL); however, hadronic showers are wider and extended up to the hadronic calorimeter (HCAL). And, muons do not produce any shower. The neutral particles are identified with the help of different parameters of showers (length, width). The neutral particle decay in to charged particles and follow V tracks.

The relevant decay channels are identified as

1. $Z^0 \rightarrow e^+e^-$
   They create electromagnetic showers through Bremsstrahlung and deposit their energy in the electromagnetic calorimeter.

2. $Z^0 \rightarrow \mu^+\mu^-$
   Muons are heaver than electrons, they don't show showers either Ecal nor Hcal. They penetrate the Hcal and trigger signal in the muon chambers.

3. $Z^0 \rightarrow \tau^+\tau-$
   Tau particles have short life time, so they decay quickly. They can be identified by their decay product. Since they are heavier than electrons and muon and their sum of momentum is less than that electrons and muons for the same energy.
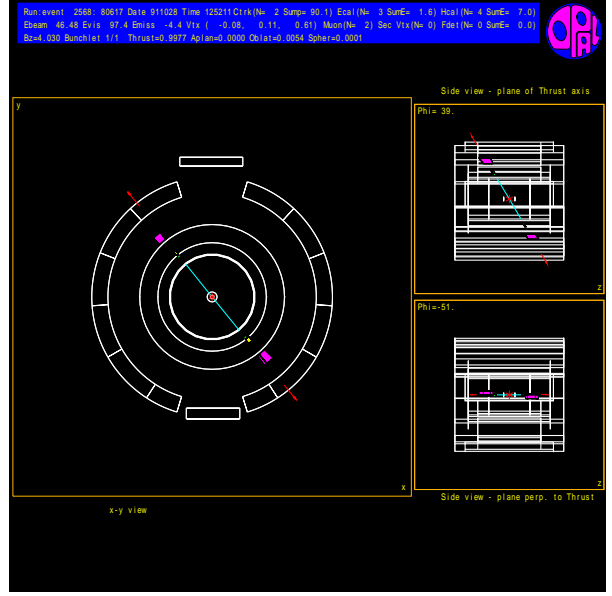
4. $Z^0 \rightarrow q\bar{q}$
   Since quarks cannot exist freely and they form jet of hadrons via strong interaction. Hadronic events have high charge tracks, so they are easy identified.

These events are also visually presented in figure 3.
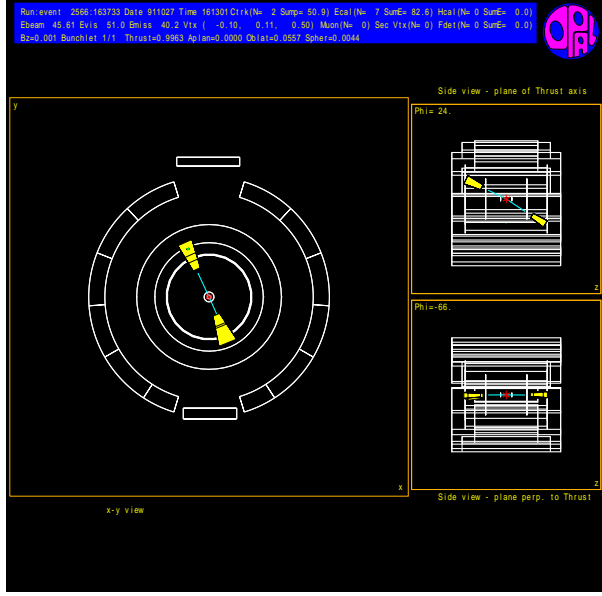
(a) $Z^0 \to e^+ e^-$

(b) $Z^0 \to \mu^+ \mu^-$
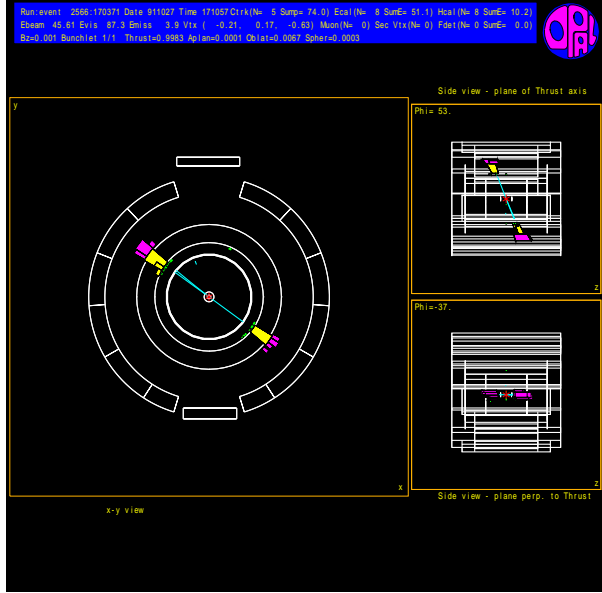
(c) $Z^0 \to \tau^+ \tau^-$
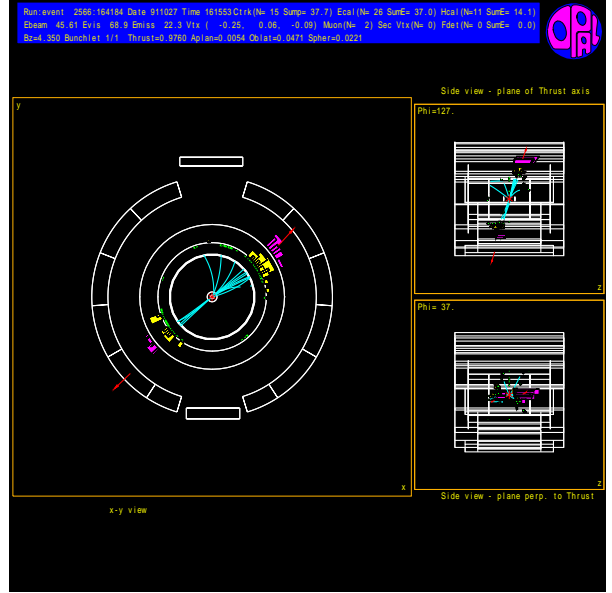
(d) $Z^0 \to q\bar{q}$

Figure 3: Four different decay modes of Z^0 boson. Here four important components of OPAL are (from inward to outward): proportional chambers, ECAL, HCAL, and muon chamber.

4.2. Determination of appropriate cuts for events classification

In this part we have access to the following variables for each event:

- `Ctrk(N)`: Number of charged tracks

- `Ctrk(SumP)`: Momentum of all charged tracks

- `Ecal(SumE)`: Total energy deposited in the electromagnetic calorimeter

- `Hcal(SumE)`: Total energy deposited in the hadronic calorimeter

The measured values for each events of channels: $Z^0 \rightarrow e^+e^-$, $Z^0 \rightarrow \mu^+\mu^-$, $Z^0 \rightarrow \tau^+\tau-$, and $Z^0 \rightarrow$ hadrons of Z^0 boson are, respectively, listed in tables 10, 11, 12, and 13 in the appendix.

We plot the histograms for different parameters of different channels and use these to choose the appropriate cuts. Figure 4 shows the histograms measured in $Z^0 \rightarrow e^+e^-$ channel.

(a) Number of charge tracks

(b) Total scalar sum of track momenta

(c) Energy deposited in the electromagnetic calorimeter

(d) Energy deposited in the hadronic calorimeter
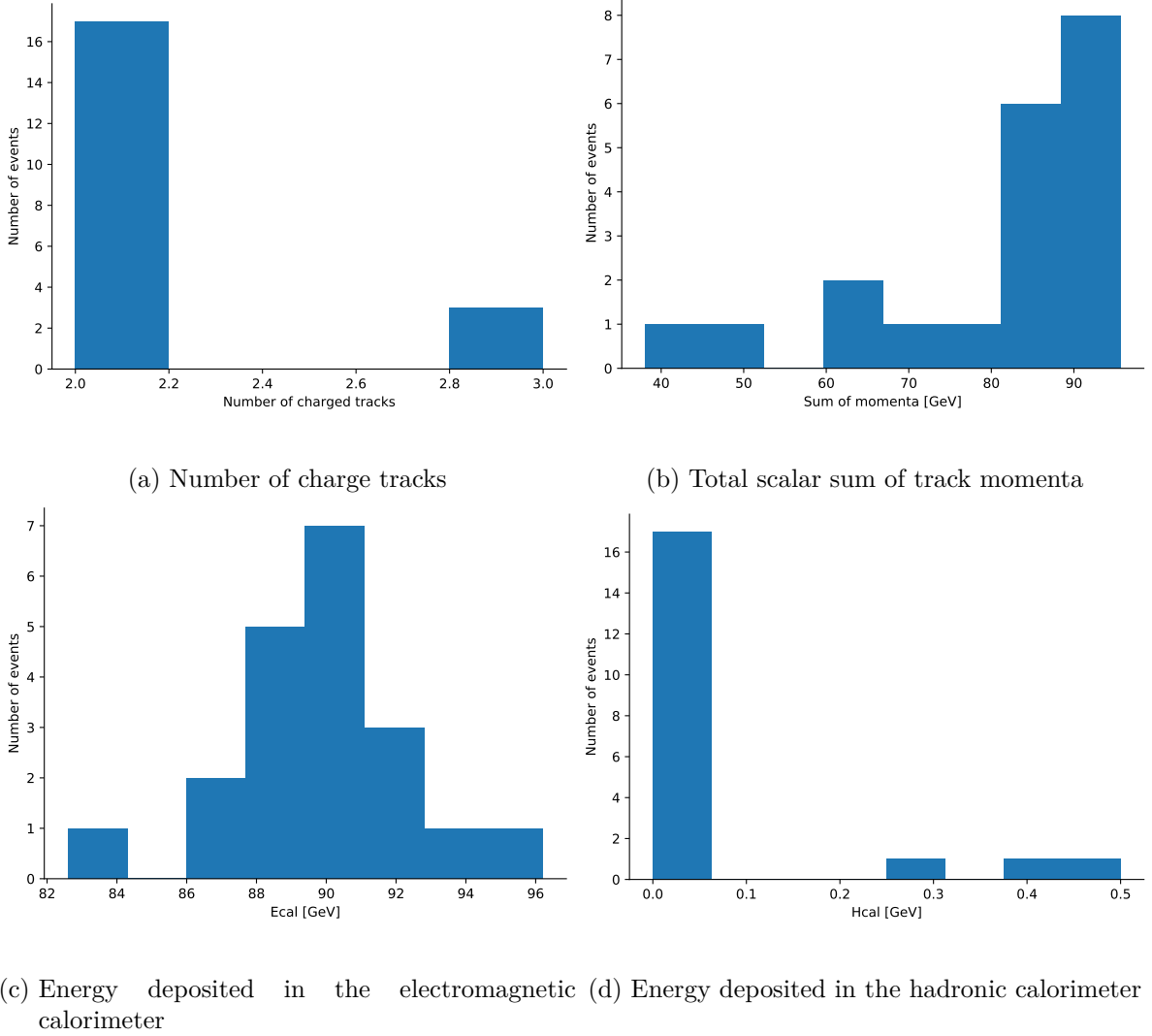
Figure 4: Histograms of different variables measured in $Z^0 \rightarrow e^+e^-$ channel.

From 4, it is clear that number of charged tracks is pretty low. Sometimes it can be higher than 2 (ideal case) because of Bremsstrahlung. From this sample, we choose the cut to be `Ctrk(N)` ≤ 3. As mentioned before, in this decay mode energy deposited in ECAL is significantly large in HCAL. Thus we demand that `Ecal(SumE)` > 50 (this will get refined anyway) and `Hcal(SumE)` < 1. Sometimes the cuts we set here leave the variable some wiggle room to

make sure good identification. There is still pattern in distribution of `Ctrk(SumP)`, but for this part we think aforementioned three cuts are more than enough.

(a) Number of charge tracks

(b) Total scalar sum of track momenta

(c) Energy deposited in the electromagnetic calorimeter

(d) Energy deposited in the hadronic calorimeter
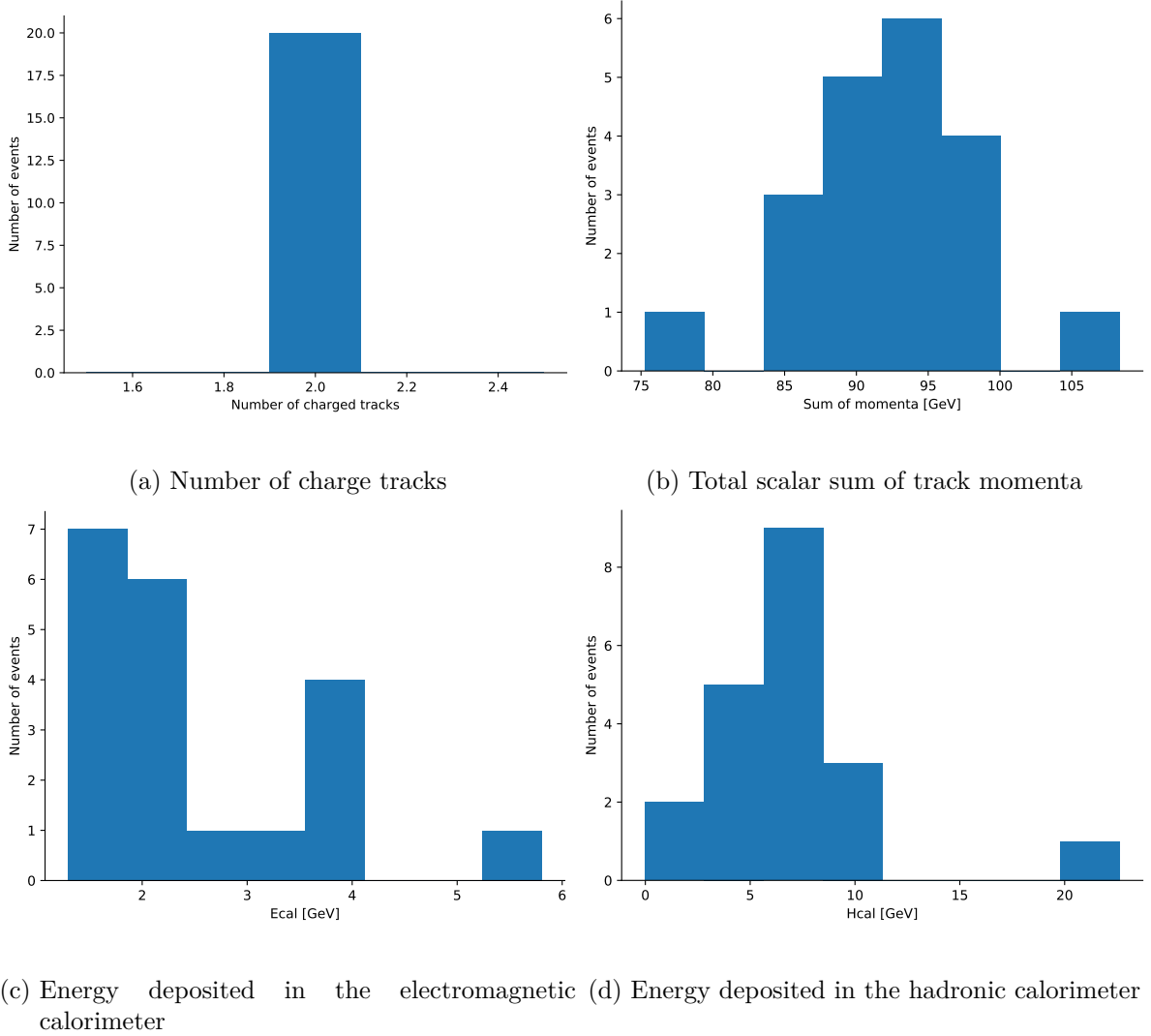
Figure 5: Histograms of different variables measured in $Z^0 \rightarrow \mu^+\mu^-$ channel.

In figure 5, four histograms are shown and these will be our basis for determining cuts. Similar as ee, number of charged track is low, thus a cut `Ctrk(N)` ≤ 3 is set. Energy of muons mostly goes to muon chamber, thus energies in ECAL and HCAl are quite low. Cuts for these two are set as `Ecal(SumE)` < 10 and `Hcal(SumE)` < 30. Here a cut in the momenta is set in order to differentiate $\mu\mu$ from $\tau\tau$: `Ctrk(SumP)` ≥ 50.

9

(a) Number of charge tracks

(b) Total scalar sum of track momenta

(c) Energy deposited in the electromagnetic calorimeter

(d) Energy deposited in the hadronic calorimeter
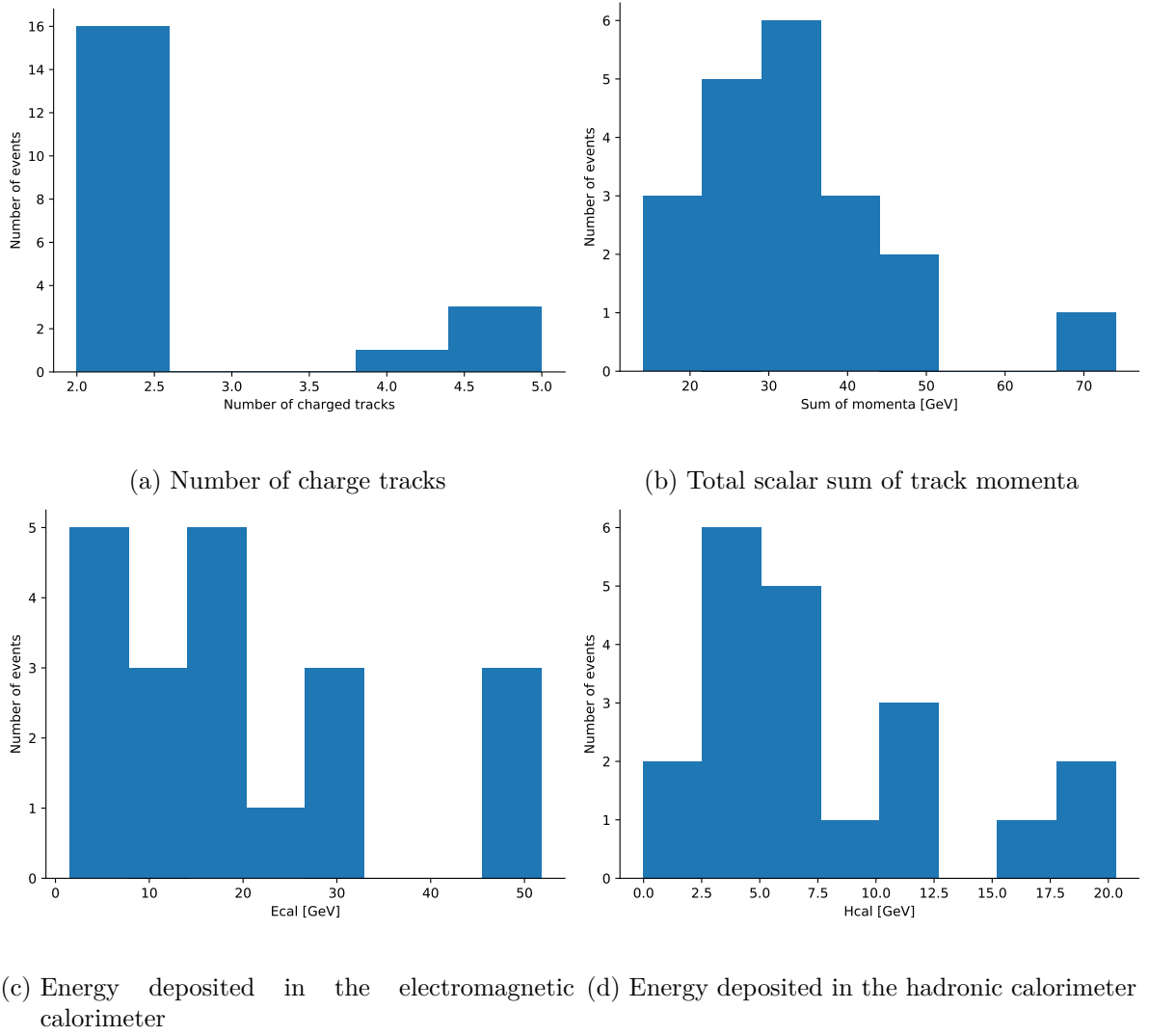
Figure 6: Histograms of different variables measured in $Z^0 \to \tau^+\tau^-$ channel.

Figure 6 shows distributions of variables in $\tau\tau$ channel. Again the number of charged track is low. But since τ can decay into charged hadrons also, we set the cut at `Ctrk(N)` ≤ 7. Two constraints on energy in ECAL and HCAL are set to `Ecal(SumE)` < 60 and `Hcal(SumE)` < 30. Compared to $\mu\mu$ channel, $\tau\tau$ has relatively low sum of momenta, thus `Ctrk(SumP)` < 75.

(a) Number of charge tracks

(b) Total scalar sum of track momenta

(c) Energy deposited in the electromagnetic calorimeter

(d) Energy deposited in the hadronic calorimeter
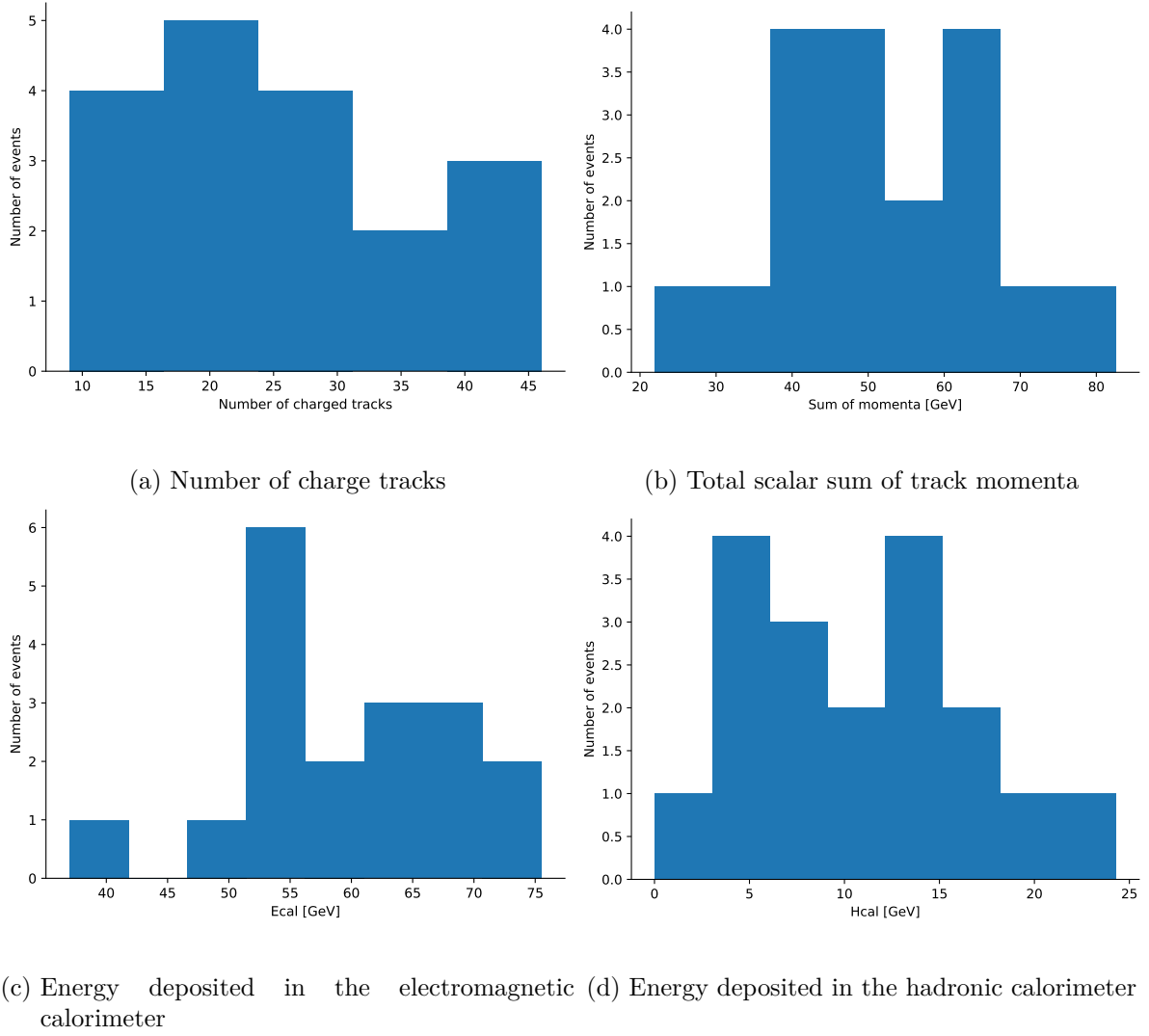
Figure 7: Histograms of different variables measured in $Z^0 \rightarrow qq$ channel.

Finally the histograms of qq channel is shown in 7. Very obvious, number of charged track is large, thus `Ctrk(N) \geq 7` is set. In principle it is enough, but we introduce another cut: `Ecal(SumE) > 30`, since we know that hadrons do deposit some energy into ECAL.

We understand there are some overlaps of cuts of $\mu\mu$ and $\tau\tau$, but this ambiguity never shows up in the test data and cuts need to improved later anyway. There are also some events potentially cannot belong to any of these categories. It is fine, as long as the corresponding cut efficiency is good. Our cuts all together are listed in table 3.

channel	Ctrk(N)	Ctrk(Sump)	Ecal(SumE)	Hcal(SumE)
ee	≤ 3		> 50	< 1
$\mu\mu$	≤ 3	≥ 50	< 10	< 30
$\tau\tau$	≤ 7	< 75	< 60	< 30
qq	≥ 7		> 30	

Table 3: Measured Cuts for different variables of different channels. Unit for energy and momenta is as always GeV.

4.3. Event classification for test sample

To classify events from the sample `test1` we used the cuts from table 3. To do so, firstly, we checked the `CtrkN` to pick out hadrons particle from others, also we verified `Ecal` number. Secondly, we check the values of `Ecal` and `Hcal` to verified electrons. Finally, we checked the value of `CtrkSump` as well as `Ecal` and `Hcal` to conform the muons or tauons. The measured valued for each variables and the decay channel classification result are given table 4.

Event	Ctrk(N)	Ctrk(Sump)	Ecal(SumE)	Hcal(SumE)	Cut classification
1	19	39.5	44.3	15.6	$Z^0 \to q\bar{q}$
2	36	42.8	57.1	12.5	$Z^0 \to q\bar{q}$
3	2	95.7	93.4	0.0	$Z^0 \to e^+e^-$
4	2	90.8	1.4	4.1	$Z^0 \to \mu^+\mu^-$
5	4	36.5	35.8	10.8	$Z^0 \to \tau^+\tau-$
6	2	97.0	2.2	8.9	$Z^0 \to \mu^+\mu^-$
7	68	42.9	48.5	6.2	$Z^0 \to q\bar{q}$
8	5	35.0	40.8	3,3	$Z^0 \to \tau^+\tau-$
9	21	75.8	45.8	21.0	$Z^0 \to q\bar{q}$
10	2	95.2	1.3	7.9	$Z^0 \to e^+e^-$
11	2	22.7	34.4	0.0	$Z^0 \to \tau^+\tau-$
12	4	44.3	37.8	2.6	$Z^0 \to \tau^+\tau-$
13	21	53.1	36.2	22.9	$Z^0 \to q\bar{q}$
14	2	89.5	92.0	0.0	$Z^0 \to e^+e^-$
15	2	89.1	89.7	0.0	$Z^0 \to e^+e^-$
16	2	4.1	4.4	0.0	$Z^0 \to \tau^+\tau-$
17	2	87.8	1.4	4.3	$Z^0 \to \mu^+\mu^-$
18	2	75.3	90.0	0.0	$Z^0 \to e^+e^-$
19	2	93.7	1.6	6.8	$Z^0 \to \mu^+\mu^-$
20	2	67.1	93.6	0.0	$Z^0 \to e^+e^-$

Table 4: Measured parameter and determined channel in test1

5. Statistical Analysis

With a large dataset, previous "event display" method will no longer be efficient and accurate. Thus data analysis tools are necessary. Here `root` is used and three macros to apply cuts are already implemented. As before we have four sets of Monte Carlo simulated data in order to find the optimal cuts, then there are a couple of real data samples.

For some reason, variables in `root` files unfortunately have different names. Here we have the same four variable and an addition parameter [2]

- `Ncharged`: number of charged tracks (`Ctrk(N)`)

- `Pcharged`: total scalar sum of track momenta (`Ctrk(SumP)`)

- `E_ecal`: total energy in electromagnetic calorimeter (`Ecal(SumE)`)

- `E_hcal`: total energy in hadronic calorimeter (`Hcal(SumE)`)

- `cos_thet`: cos(polar angle) between incoming positron and outgoing positive particle
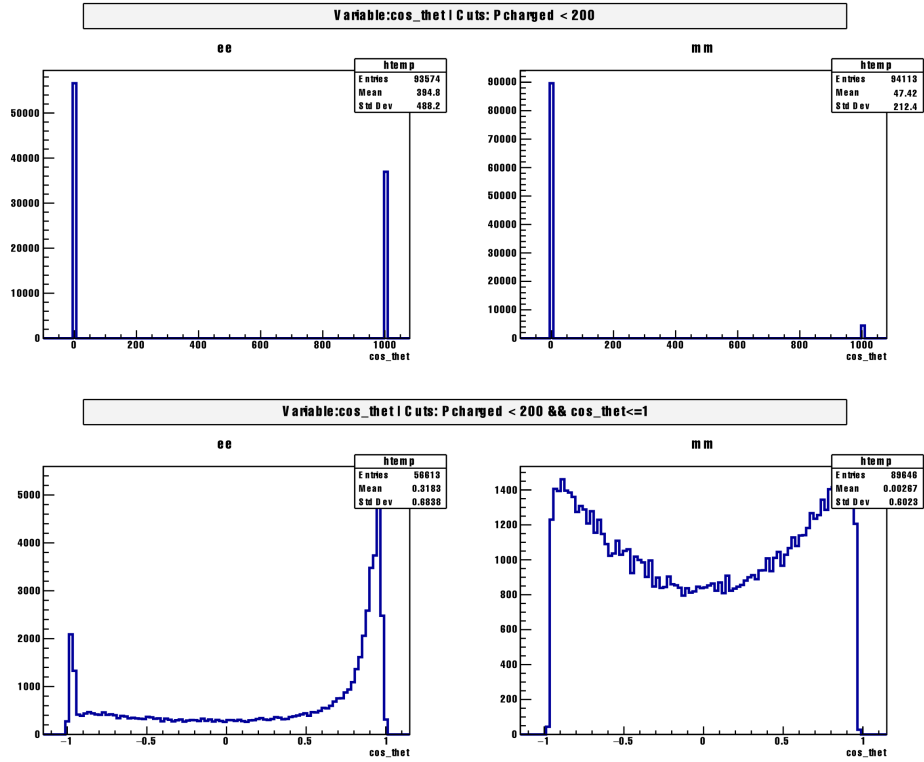
5.1. Mode selection

Figure 8: Distribution of `cos_thet` before and after `cos_thet` cut.

First of all, there are a couple of general cuts. The collider energy of LEP is $\sim 200\,\text{GeV}$. Thus the scalar sum of momenta should be maximally around this value. Events with even larger momenta are caused by various unphysical processes. Secondly, the data here is written such as

when there are multiple outgoing positive particles, `cos_thet` = 1000. For ee and $\mu\mu$ process, it should not be possible, since no hadronisation can occur and initial/final state radiation for these two only involve photons. So for these two event selections, cut `cos_thet <= 1.0` is applied, see figure 8. After the cut(s), there are 56613 ee events, 89646 $\mu\mu$ events, 79099 $\tau\tau$ events, and 98100 qq events.

In event display part, we have success using cut `Ncharged > 7` for qq processes. We conclude that this is no longer sufficient, since there are quite many $\tau\tau$ contamination, see figure 9. While roughly 5% percent of qq events are lost, $\tau\tau$ events are barely present and ee, $\mu\mu$ are completely cut. So the 5% percent are considered as acceptable "casualties". We drop the cut in `E_ecal`. After the cut for qq, no ee or $\mu\mu$ are left, 78 $\tau\tau$ survives and 92688 qq events remain.

Follow the same receipt as in event display part, we try to separate ee events from other leptonic channels. Cut in number of charged track remains the same: `Ncharged` < 4 or (≤ 3). Same as before `E_ecal` of ee events have peak at around $80\,\mathrm{GeV}$. `E_ecal` cut is changed to `E_ecal > 60`, since there is virtually no events even at `E_ecal = 60`, see figure 10. `E_hcal` cut is similar to before, just relaxed a little bit (to `E_hcal < 2`), since some of events have higher `E_hcal` as previous cut, see figure 11. In the end, we end up with 51679 ee events, 0 $\mu\mu$, 910 $\tau\tau$ events, and 1 qq event.

For $\mu\mu$ selection, cut in `Ncharged` is the same as ee: `Ncharged` < 4. We have already seen in figure 10 that `E_ecal` of $\mu\mu$ has a peak around 0, so the `E_ecal` cut for ee gets inverted as cut for $\mu\mu$: `E_ecal` < 60. Then remaining $\tau\tau$ events can be excluded with the help of `Pcharged`, see figure 12. ee and qq events are basically cut away, only unwanted events are $\tau\tau$. `Pcharged` distributions of $\mu\mu$ and $\tau\tau$ are separated quite nicely, although some $\mu\mu$ events have `Pcharged` ≈ 0. A cut at `Pcharged > 70` will remove most of $\tau\tau$ events while preserve most of $\mu\mu$ events. After combinations of these cuts, 144 ee events, 83228 $\mu\mu$ events, 480 $\tau\tau$ events and zero qq event survive.

$\tau\tau$ can be picked out using the same cuts for $\mu\mu$ expect `Pcharged` cut gets inverted. Since there is a small peak at `Pcharged` = 0 in ee and $\mu\mu$ events, see figure 12, a lower bound in `Pcharged` should be set as well. Thus for $\mu\mu$: 1 < `Pcharged` < 60. E_ecal cut should be adjusted a bit. In figure 10, there are still quite substantial amount of $\tau\tau$ event between 60 < `E_ecal` < 70. Thus we have for $\tau\tau$: `E_ecal` < 70. Cut in `Ncharged` is relaxed to < 5 for better efficiency. After all these cuts, we have 243 ee events, 1446 $\mu\mu$ events, 66990 $\tau\tau$ events, and 38 qq events.

All the cuts are summarizes in table 5

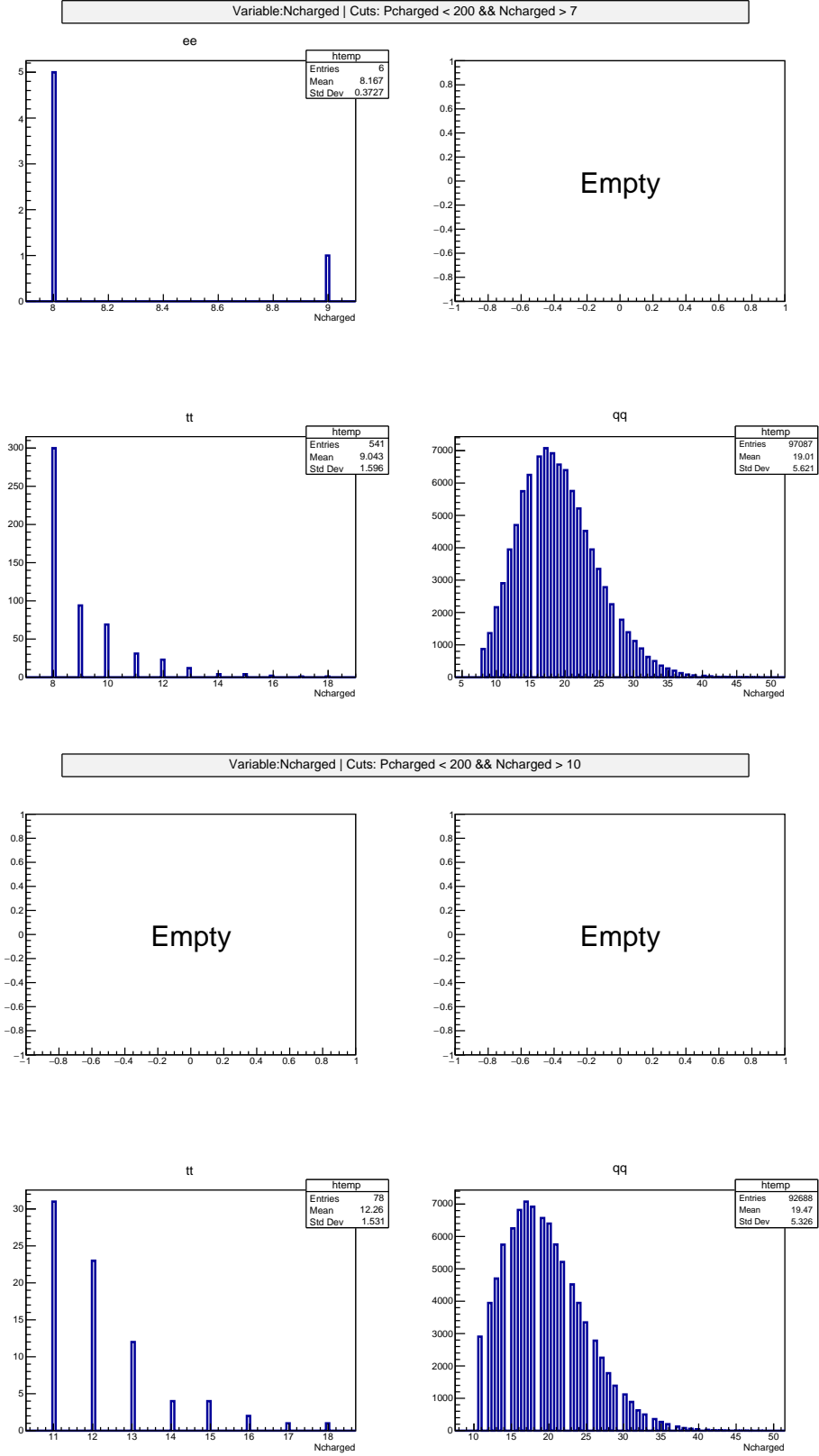| mode	cos_thet	Pcharged	Ncharged	E_ecal	E_hcal
ee	≤ 1	< 200	< 4	> 60	< 2
$\mu\mu$	≤ 1	$> 70, < 200$	< 4	< 60	
$\tau\tau$		$> 1, < 60$	< 5	< 70	
qq		< 200	> 10		

Table 5: All cuts applied to select decay modes

14

Figure 9: Number of charged tracks (`Ncharge`) before and after the refined cut for *qq* events.
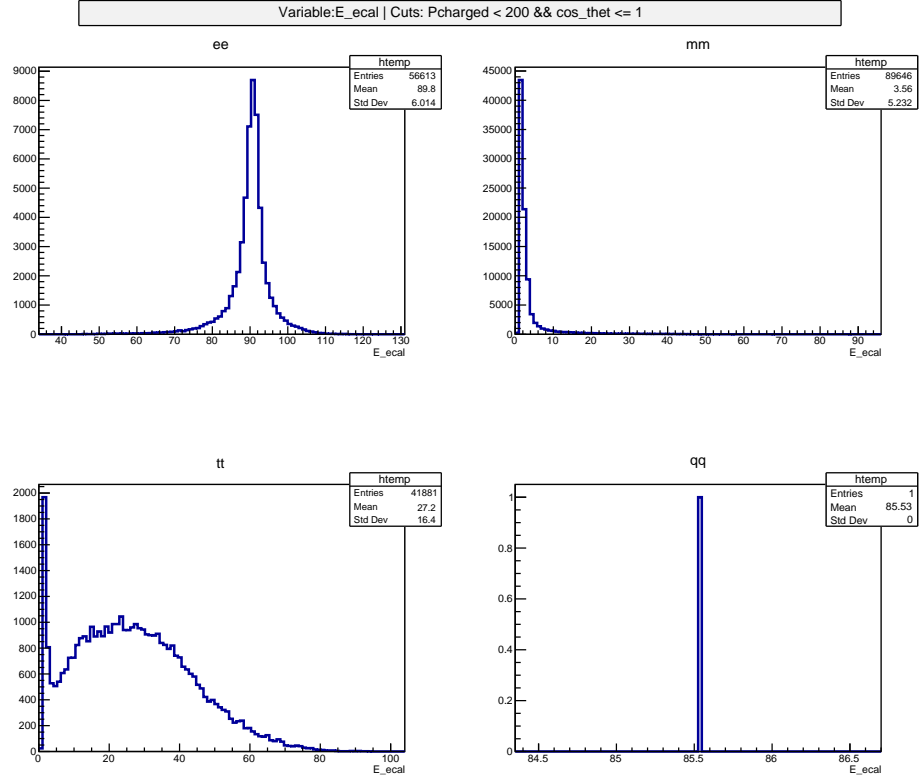
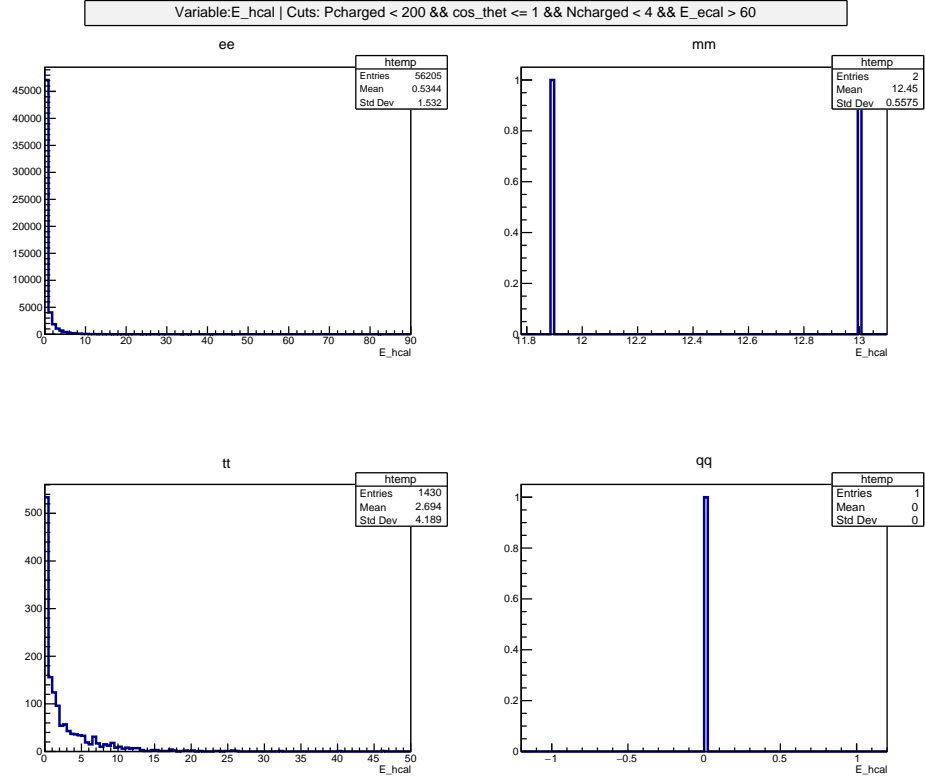Figure 10: `E_ecal` distribution before `E_ecal` cut for *ee*.

Figure 11: `E_hcal` distribution after `E_ecal` but before `E_hcal` cut for *ee*.
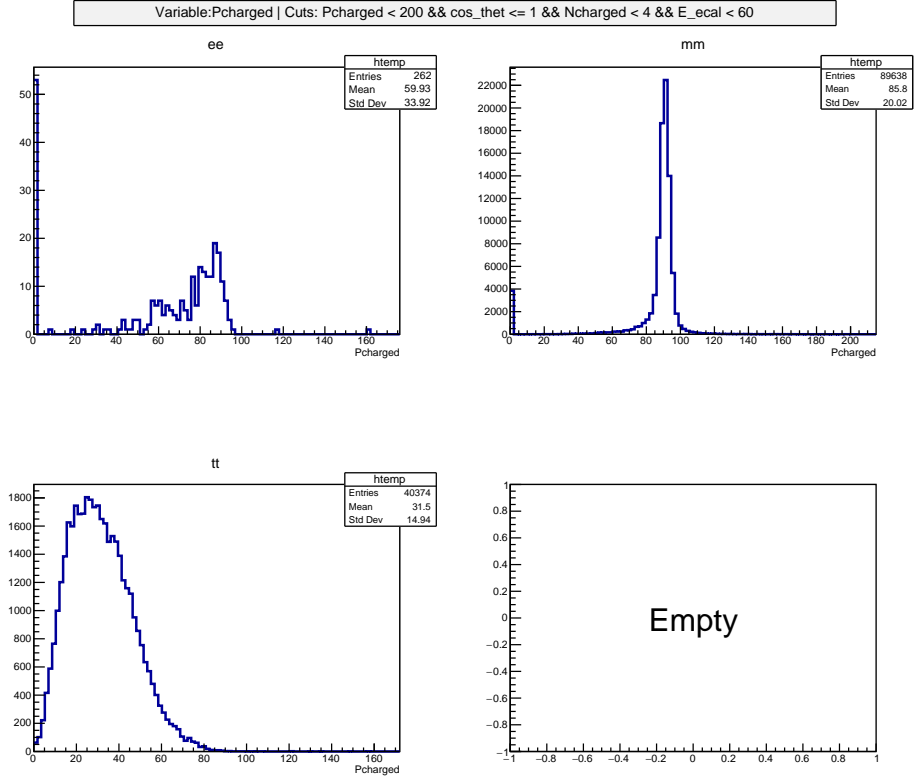
Figure 12: `Pcharged` distribution after `E_ecal` cut for $\mu\mu$.

5.2. Channel selection

Since processes with e^+e^- as final states include also t-channel elastic scattering between electron and positron and they are irrelevant processes in our discussion, we want to somehow get rid of these contributions. From figure 2 in pre-lab tasks, we know that s-channel dominates at small $\cos\Theta$ and s-channel contributions should look like symmetric around $\cos\Theta = 0$. Naturally, first thing comes in our minds is to cut $\cos\Theta$ from somewhere between 0 and 1 to $-\infty$, so that it looks symmetric. Figure 13 is done with $\cos\Theta < 0.5$. There is a quite significant peak around $\cos\Theta = -1$, which we don't really expect. Physical origin of this peak is unknown to us, but anyway this should be cut away. In the end, we have the cut $-0.9 < \cos\Theta < 0.5$. This cut along with the previous *ee* cuts will be the new *ee* cuts used onwards.
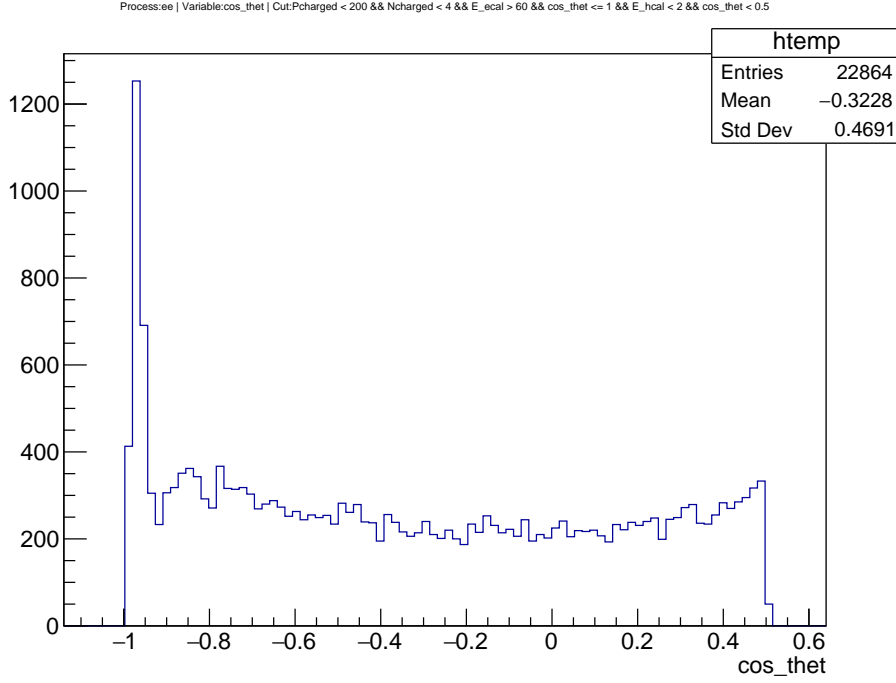
Figure 13: $\cos\Theta$ distribution of *ee* events after previously determined *ee* cuts and $\cos\Theta < 0.5$.

5.3. Forward-backward asymmetry

Numbers of events in forward $(0 < \cos\theta < 1)$ and backward $(-1 < \cos\theta < 0)$ are measured using `data1.root` and MC data with $\mu\mu$ as final states. In the actual analysis, only the real data are used. Upon inspection of definition 6, it is clear that correction for cut efficiency is unnecessary here, since $N_{+,-}$ share the same cuts.

After application of equation 6 at all available CMS energy, correction terms should be added to the measured asymmetry. As we understand it, applying these corrections will remove radiation corrections in measured data, so that we can directly compare experimental values with tree-level theoretical values.

Figure 14 shows the forward-backward asymmetry at various CMS energies. Errors are calculated as usual $\sigma_N \approx \sqrt{N}$.
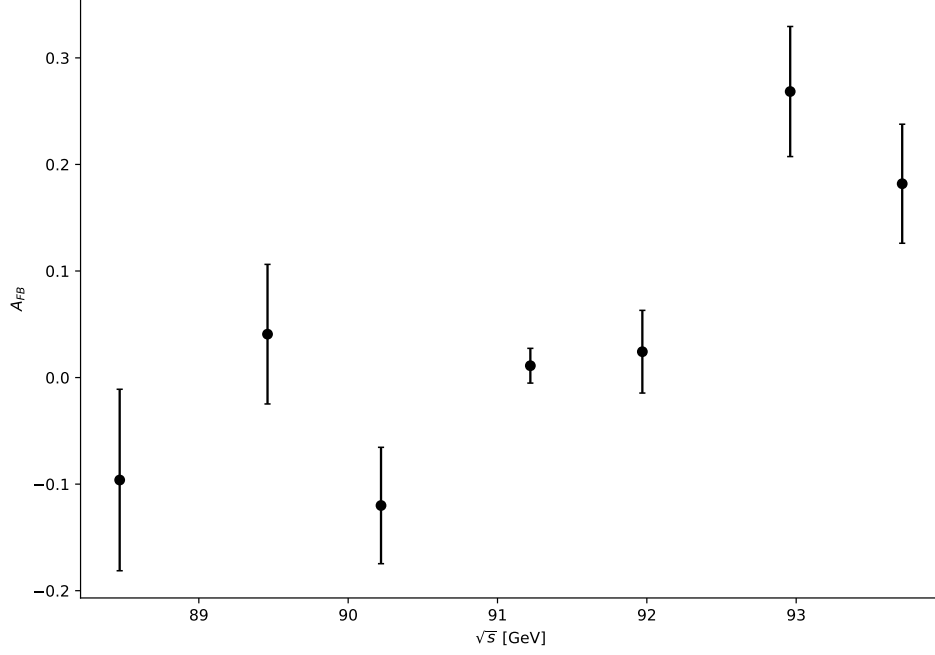
Figure 14: Forward-backward asymmetry after applying corrections.

If one says that the fourth data point (with $\sqrt{s} = 91.22\,\text{GeV}$) lies *exactly* at the peak of resonance, this A_{FB} can be used to determined the Weinberg angle from equation 8

$$\sin^2 \theta_W = \frac{1 - \sqrt{A_{\text{FB}}^{\mu,\text{peak}}/3}}{4}$$
$$\sigma_{\sin^2 \theta_W} = \frac{1}{8\sqrt{3}} \frac{\sigma_A}{\sqrt{A}}$$

Then we have

$$\sin^2 \theta_W = 0.2347 \pm 0.0112 \tag{16}$$

From PDG [3], in $\overline{\text{MS}}$ and $\sqrt{s} = M_Z$, the angle is $\sin^2 \theta_W = 0.231\,21 \pm 0.000\,04$. Our value matches it quite well.

In principle one can calculate the Weinberg angle at every CMS energy using equation 7. But then according to QFT, value of Weinberg angle also changes, since it depends on the coupling g and g'. Thus we just settle with this value as our final result.

5.4. Cut efficiency

Cut efficiency can be defined as

$$\epsilon_{ij} = \frac{N_i}{N_j} \tag{17}$$

where a cut i is applied to a process j. In previous sections, there are multiple cuts and MC simulation data. By applying all the cuts to all the data, a 4×4 efficiency matrix can be

obtained

$$\epsilon = \begin{pmatrix} N_{ee,\text{cuts}}/N_{ee} & N_{ee,\text{cuts}}/N_{\mu\mu} & N_{ee,\text{cuts}}/N_{\tau\tau} & N_{ee,\text{cuts}}/N_{qq} \\ N_{\mu\mu,\text{cuts}}/N_{ee} & N_{\mu\mu,\text{cuts}}/N_{\mu\mu} & N_{\mu\mu,\text{cuts}}/N_{\tau\tau} & N_{\mu\mu,\text{cuts}}/N_{qq} \\ N_{\tau\tau,\text{cuts}}/N_{ee} & N_{\tau\tau,\text{cuts}}/N_{\mu\mu} & N_{\tau\tau,\text{cuts}}/N_{\tau\tau} & N_{\tau\tau,\text{cuts}}/N_{qq} \\ N_{qq,\text{cuts}}/N_{ee} & N_{qq,\text{cuts}}/N_{\mu\mu} & N_{qq,\text{cuts}}/N_{\tau\tau} & N_{qq,\text{cuts}}/N_{qq} \end{pmatrix} \tag{18}$$

$$= \begin{pmatrix} 0.9667 \pm 0.0096 & 0.0000 \pm 0.0000 & 0.0082 \pm 0.0003 & 0.0000 \pm 0.0000 \\ 0.0070 \pm 0.0006 & 0.9284 \pm 0.0045 & 0.0061 \pm 0.0003 & 0.0000 \pm 0.0000 \\ 0.0153 \pm 0.0009 & 0.0317 \pm 0.0006 & 0.8881 \pm 0.0046 & 0.0004 \pm 0.0001 \\ 0.0000 \pm 0.0000 & 0.0000 \pm 0.0000 & 0.0010 \pm 0.0001 & 0.9448 \pm 0.0043 \end{pmatrix}$$

Raw data can be found in appenfix A.2. Note that the total number of events considered here is the number *after* the general `Pcharged` and `cos_thet` (including *s*-channel selection) cuts. After all, cuts efficiencies we discuss here are only the efficiencies of cuts like *ee* cuts and so on.

Error is estimated using Poisson statistic and usual error propagation formula

$$\sigma_{\epsilon_{ij}} = \sqrt{\left(\frac{1}{N_j} \sigma_{N_i} \right)^2 + \left(\frac{N_i}{N_j^2} \sigma_{N_j} \right)^2} = \sqrt{\frac{N_i}{N_j^2} + \frac{N_i^2}{N_j^3}}$$

Actually the $\epsilon_{i,ee}$ efficiencies are problematic, because in `cos_thet` cuts, one part of *s*-channel gets lost. Main purpose of efficiency matrix is to obtain true number of events from measured number of events. If we continue to use $\epsilon_{i,ee}$ without further corrections, the true number of events are of $-0.9 < $ `cos_thet` < 0.5, resulting lower counts.

The correction involves adjustment of denominator or $\epsilon_{i,ee}$, since in selecting N_{ee} the *s*-channel cuts are applied. For this, the function $(1 + \cos^2 \Theta)$ is integrated in $-0.9 < \cos \Theta < 0.5$ and in $-1 < \cos \Theta < 1$.

$$\text{corr. factor} = \frac{\int_{-1}^{1} \mathrm{d}x \, (1 + x^2)}{\int_{-0.9}^{0.5} \mathrm{d}x \, (1 + x^2)} \approx 1.583 \tag{19}$$

This number is then multiplied to all the denominator of first column in equation 18. Now the corrected efficiency matrix is

$$\epsilon = \begin{pmatrix} 0.6107 \pm 0.0061 & 0.0000 \pm 0.0000 & 0.0082 \pm 0.0003 & 0.0000 \pm 0.0000 \\ 0.0044 \pm 0.0004 & 0.9284 \pm 0.0045 & 0.0061 \pm 0.0003 & 0.0000 \pm 0.0000 \\ 0.0097 \pm 0.0006 & 0.0317 \pm 0.0006 & 0.8881 \pm 0.0046 & 0.0004 \pm 0.0001 \\ 0.0000 \pm 0.0000 & 0.0000 \pm 0.0000 & 0.0010 \pm 0.0001 & 0.9448 \pm 0.0043 \end{pmatrix} \tag{20}$$

5.5. Partial cross sections

From last section, cut efficiency matrix is obtained. It describes how true numbers of events T_i translate into measured numbers of events M_i, i.e.

$$\mathbf{M} = \epsilon \mathbf{T} \tag{21}$$

In this compact matrix notation, $\mathbf{M}$ and $\mathbf{T}$ are vectors containing the numbers of events in a decay mode. Entries of $\mathbf{T}$ are listed in table 15 in appendix.

With real data in `data1.root`, we have the measured numbers using the cuts defined earlier. To find out true numbers, one needs to find inverse matrix ϵ^{-1}.

$$\mathbf{T} = \epsilon^{-1}\mathbf{M} \tag{22}$$

We can propagate errors in ϵ and $\mathbf{M}$ to obtain an accurate error estimation of $\mathbf{T}$. According to [4],

$$\text{Cov}(\epsilon_{ab}^{-1}, \epsilon_{cd}^{-1}) = ([\epsilon^{-1}]_{ai}[\epsilon^{-1}]_{ci})[\sigma_\epsilon]_{ij}^2([\epsilon^{-1}]_{jb}[\epsilon^{-1}]_{jd}) \tag{23}$$

and the correlation matrix of $\mathbf{T}$ is

$$\text{Cov}(T_i, T_j) = M_\alpha M_\beta \text{Cov}(\epsilon_{i\alpha}^{-1}, \epsilon_{j\beta}^{-1}) + \epsilon_{ik}^{-1}\epsilon_{jl}^{-1}\text{Cov}(M_k, M_l) \tag{24}$$

where $\text{Cov}(M_k, M_l)$ is covariance matrix for measured counts and generally diagonal. This a bit complicated formula should be used instead of ignoring uncertainties in ϵ. We have tested that simplification will lead to at least 50% under-estimation of the errors.

After correction for efficiency, number of events needs to be divided by integrated luminosity $L = \int \mathrm{d}t\,\mathcal{L}$ to obtain partial differential cross section (values listed in table 16 in appendix). To account for higher order of Feynman diagrams, radiative corrections are added to the final results. They are listed in table 6

$\sqrt{s}$ [GeV] / σ_i[nb]	ee	$\mu\mu$	$\tau\tau$	qq
88.47	0.389 ± 0.028	0.304 ± 0.018	0.338 ± 0.021	7.260 ± 0.094
89.46	0.791 ± 0.043	0.656 ± 0.030	0.602 ± 0.030	14.105 ± 0.146
90.22	1.221 ± 0.060	1.196 ± 0.047	0.980 ± 0.043	25.744 ± 0.230
91.22	1.718 ± 0.032	1.805 ± 0.022	1.619 ± 0.022	40.578 ± 0.175
91.97	1.094 ± 0.050	1.328 ± 0.044	1.107 ± 0.041	28.804 ± 0.231
92.96	0.458 ± 0.041	0.562 ± 0.036	0.541 ± 0.037	13.721 ± 0.188
93.71	0.323 ± 0.030	0.362 ± 0.025	0.308 ± 0.025	8.102 ± 0.125

Table 6: Partial cross section for various decay modes

Here the partial cross section is calculated with

$$\boldsymbol{\sigma} = \mathbf{L}^{-1}\mathbf{T} \tag{25}$$

where $\boldsymbol{\sigma}$ is vector like $\mathbf{T}$ and luminosity has been "promoted" to be a (diagonal) matrix $\mathbf{L}$. So formula 24 can be used to calculate covariance matrix of partial cross sections. In table 6, errors are propagated using only diagonal entries (variance) of the covariance matrix.

Figure 15 shows the partial cross sections of leptonic decay channels. Three curves are quite similar. From the numerical values in table 6, one can see that the leptonic partial cross sections at peak ($\sqrt{s} = 91.22\,\text{GeV}$) differ from each other at $\sim 2\sigma$'s. Leptonic universality states that except mass difference, three generations of leptonic should behave the same. At such high energy ($\sqrt{s} \approx 90\,\text{GeV}$), lepton masses are negligible and the partial cross sections should be identical. Here we do see some differences. This could be caused by some systematic regarding detection of one or more of the leptonic channels.

Partial cross sections to hadronic end states are quite high, because of the colour charge. Their partial cross sections are plotted in figure 16.
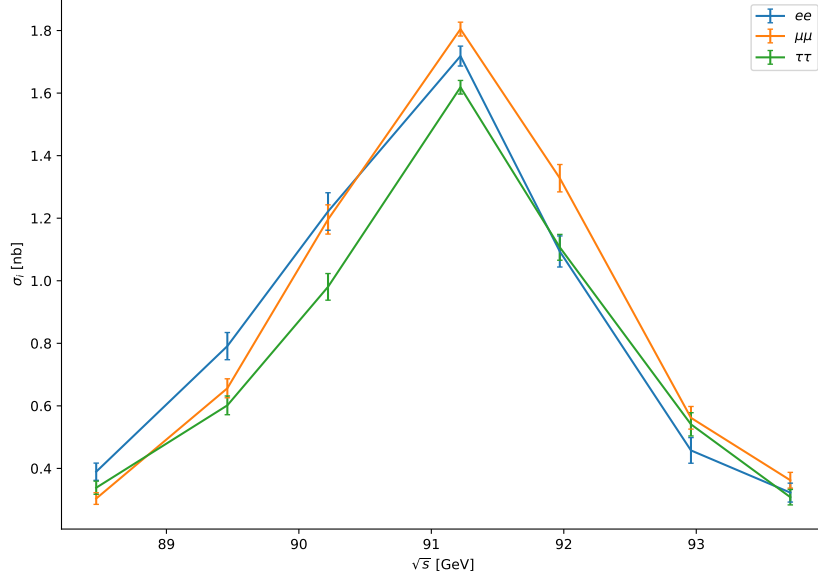
Figure 15: Partial cross section in leptonic channels

To compare theory and our measurement, one can try to calculate the ratios of hadronic cross section to (total) leptonic cross section. From the data, we have

$$\left[\frac{\sigma_{\text{had}}}{\sigma_{\text{lep}}}\right]_{\text{exp}} = 7.892 \pm 0.076 \tag{26}$$

whereas the theory predicts

$$\left[\frac{\sigma_{\text{had}}}{\sigma_{\text{lep}}}\right]_{\text{theo}} = 6.692 \tag{27}$$

The measured value is quite off from the prediction, meaning it is not very likely that statistical fluctuations will explain this. A possible cause of this is the error could be underestimated somehow. Other factors like detection efficiencies and Monte Carlo simulation quality can play a role.

Actually this calculation can be misleading and inaccurate. With formula 24, we see that there should be correlation of different channels to some extent. But when calculating the ratio, this correlation is not considered. Instead, it would be better to draw 1σ, 2σ etc. circles on σ_{had}-σ_{lep} plane and see where the theoretical value lies. We reckon that it will not change the result too much and decide not to proceed with this method.

5.6. Breit-Wigner fit

For all decay modes, there is a clear peak at $\sqrt{s} = M_Z \approx 91\,\text{GeV}$, where the partial cross sections increase drastically. This behaviour can be modelled with the Breit-Wigner form 2, where Γ_e, Γ_f, M_Z and Γ_Z are the to be determined fit parameters. According to CERN documentation [5], the actual shape of curve might be a convolution of Breit-Wigner and Gaussian function, depending on the detector resolution. Here we will proceed with simple Breit-Wigner form.
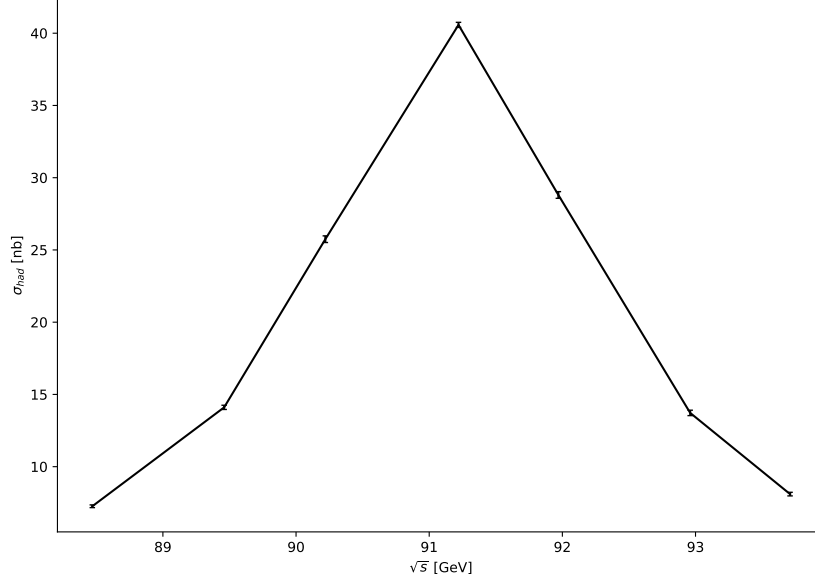
Figure 16: Partial cross section in hadronic channels

Since we have only 7 data points but 4 fit parameters for one channel, we should not expect the fit quality to be high (degrees of freedom 3). (One can improve the fit by making $\Gamma_e \cdot \Gamma_f$ into a fit parameter, so that degrees of freedom decreases by 1.) Actually, `curve_fit` method in `scipy` cannot give reliable estimation of covariance matrix involving Γ_e and Γ_f. This can be caused by high condition number [6]. This leads to a problem that errors of Γ_e and Γ_f cannot be provided in the fitting process. It should not be a big issue, since in this step we want to find out the Z^0 width and peak only. Also the errors in σ_i are always from the diagonal entries of the covariance matrix, since the covariance matrices represent correlation of different cross sections at one certain CMS energy but here we plot one σ_i at all CMS energies (otherwise one could input the appropriate covariance matrix into `curve_fit`).

channel	Γ_e[MeV]	Γ_f[MeV]	Γ_Z[GeV]	M_Z[GeV]	$\sigma_{i,\text{peak}}$[nb]
ee	84.568	77.060	2.551 ± 0.106	90.972 ± 0.033	$1.777^{+0.159}_{-0.141}$
$\mu\mu$	84.209	77.171	2.513 ± 0.066	91.166 ± 0.029	$1.818^{+0.101}_{-0.093}$
$\tau\tau$	78.267	76.439	2.559 ± 0.111	91.151 ± 0.029	$1.615^{+0.151}_{-0.132}$
qq	93.619	1565.958	2.526 ± 0.025	91.193 ± 0.008	$40.584^{+0.832}_{-0.810}$

Table 7: Fit parameters and peak partial cross sections.

There are multiple Γ_Z's and M_Z's from the fitting, these values need to get averaged

$$M_Z = (91.118 \pm 0.013)\,\text{GeV} \tag{28}$$
$$\Gamma_Z = (2.537 \pm 0.042)\,\text{GeV} \tag{29}$$

24

(a) $Z^0 \to ee$ partial cross section

(b) $Z^0 \to \mu\mu$ partial cross section

(c) $Z^0 \to \tau\tau$ partial cross section

(d) $Z^0 \to qq$ partial cross section
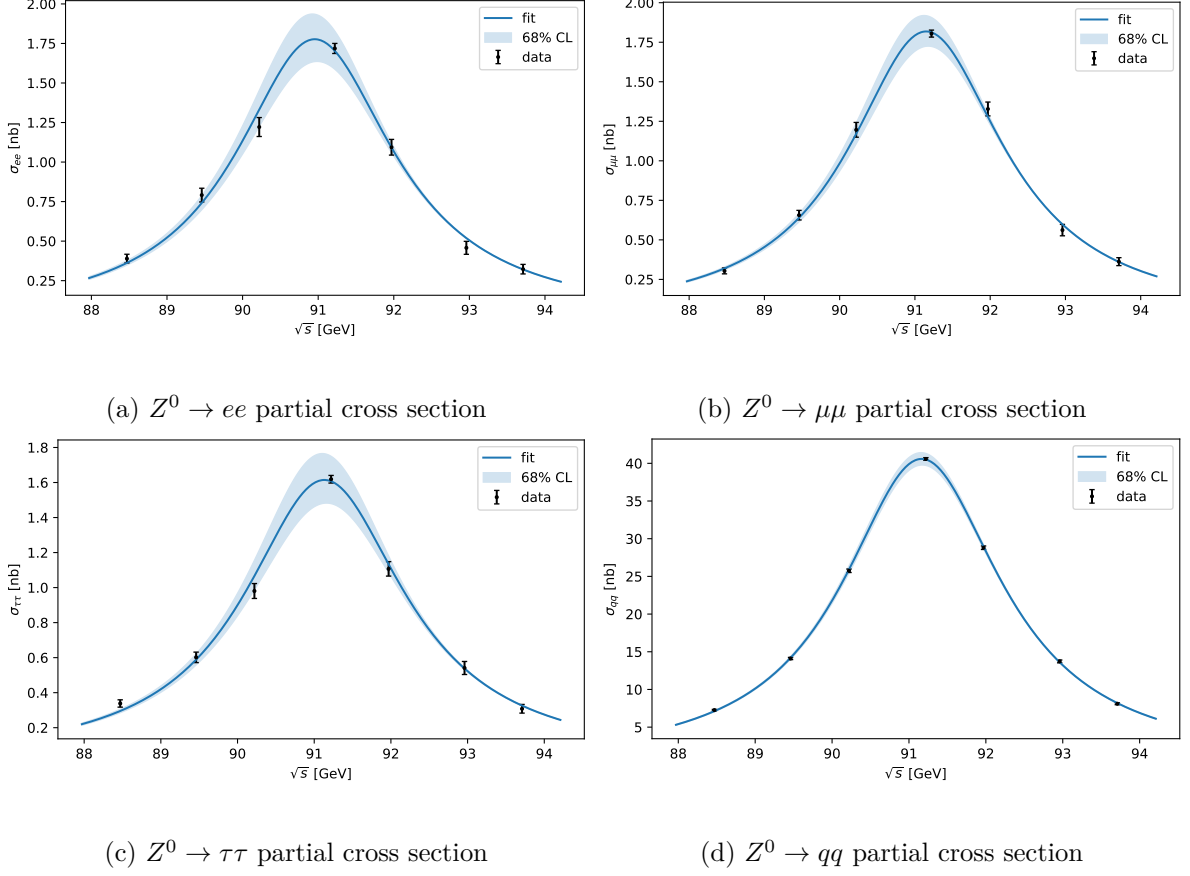
Figure 17: Partial cross section of all (visible) channels along with fit. Here the "68%" CL regions are drawn only using the errors in Γ_e and M_Z, since no errors in Γ_e and Γ_f can be reliably determined.

where the errors are propagated to be something like quadratic mean(same for both quantities)

$$\sigma_{\Gamma_Z} = \frac{1}{N} \sqrt{\sum^N \sigma^2_{\Gamma_Z, i}}$$

PDG gives $M_Z = (91.1876 \pm 0.0021)\,\text{GeV}$ and $\Gamma_Z = (2.4952 \pm 0.0023)\,\text{GeV}$ as their best fit [3]. It tells us our value of Γ_Z is more or less consistent with theirs, whereas M_Z lie a bit further from the literature values.

In order to test the goodness of our result, a χ^2 test is performed. First of all, χ^2 is computed with

$$\chi^2 = \sum_{k=1}^{N} \frac{(O_k - E_k)^2}{\sigma_k^2} \tag{30}$$

where O_k is the observed values, E_k the expected values and σ_k is the standard deviation (assuming Gaussian distribution) [7]. Degree of freedom is 3. Then these two values are plugged in CDF of χ^2 distribution to obtain the so-called p-value.

χ^2 and p-values for each datasets are listed in table 8. p-value represents the probability to obtain results as extreme or more extreme than the already observed one. By that bigger

channel	χ^2	p value
ee	8.153	0.043
$\mu\mu$	3.804	0.283
$\tau\tau$	9.652	0.022
qq	4.333	0.228

Table 8: χ^2 and p-value for each channel

numbers are better in the sense that the results as extreme or more extreme are quite likely to be reproduced. Then we see that $\mu\mu$ and qq have good p-values, whereas the others don't. ee channel is inherently contaminated by t-channel elastic contributions, so data with relatively poor quality is expected. $\tau\tau$ may involves some messy QCD processes, which can cause the problem here. As mentioned before, the fit model can be improved with convolution of Gaussian and Breit-Wigner functions to take detection resolution into account.

5.7. Partial width

Partial widths can be easily determined given width and mass of Z^0, partial cross section at peak and width to ee, see equation 3. All except width to ee are known from fitting.

One may notice that the errors in $\sigma_{i,\text{peak}}$ are asymmetrical, i.e. not Gaussian. Here to simplify thins, we assume they are still Gaussian and just take mean value of upper and lower bounds to form standard deviations.

Γ_e should be first determined out of all widths by looking at $\sigma_{e,\text{peak}}$

$$\Gamma_e = \sqrt{\frac{\sigma_{e,\text{peak}}}{12\pi}} M_Z \Gamma_Z \tag{31}$$

The error is calculated with

$$\sigma_{\Gamma_e}^2 = \Gamma_e^2 \left[\left(\frac{\sigma_{\sigma_{e,\text{peak}}}}{2\sigma_{e,\text{peak}}} \right)^2 + \left(\frac{\sigma_{\Gamma_Z}}{\Gamma_Z} \right)^2 + \left(\frac{\sigma_{M_Z}}{M_Z} \right)^2 \right]$$

With Γ_e, other partial widths can be obtained using

$$\Gamma_f = \frac{\sigma_{f,\text{peak}}}{12\pi} M_Z^2 \Gamma_Z^2 \frac{1}{\Gamma_e} \tag{32}$$

Now the errors are

$$\sigma_{\Gamma_f}^2 = \Gamma_f^2 \left[\left(\frac{\sigma_{\sigma_{f,\text{peak}}}}{\sigma_{f,\text{peak}}} \right)^2 + \left(\frac{2\sigma_{M_Z}}{M_Z} \right)^2 + \left(\frac{2\sigma_{\Gamma_Z}}{\Gamma_Z} \right)^2 + \left(\frac{\sigma_{\Gamma_e}}{\Gamma_e} \right)^2 \right]$$

Measured values along with values from PDG are listed in table 9. They are consistent with each other, except $_\tau$. Our values have quite high uncertainties. This can be traced back to poor quality of fits and the fit parameters have high uncertainties.

	measured[MeV]	PDG[MeV]
Γ_e	80.426 ± 3.648	83.91 ± 0.12
Γ_μ	82.297 ± 6.382	83.99 ± 0.18
Γ_τ	73.083 ± 7.610	84.08 ± 0.22
Γ_q	1836.996 ± 109.893	1744.4 ± 2.0

Table 9: Comparison of measured partial widths and partial widths from PDG [3]

5.8. Generations of light neutrinos

From previous section, we have collected total decay width of Z^0 and visible partial decay width of Z^0. The difference is the invisible partial width, which should consists of $Z^0 \to \nu\bar{\nu}$ processes.

$$\Gamma_{\mathrm{inv}} = (464.195 \pm 70.050)\,\mathrm{MeV} \tag{33}$$

Assuming decay width of Z^0 to single generation of neutrino is exactly as the theory predicts, like in equation 10. Then we have the number of neutrino generations

$$N_\nu = 2.799 \pm 0.422 \tag{34}$$

6. Conclusion and outlook

In this report, we have made up our cuts for different decay channels of Z^0. Using these cuts, we can count the number of events in one specific decay channel and thus calculate the cross section using luminosity values.

By looking at final states in forward and backward direction, the so-called forward-backward asymmetry is determined and this value is directly related to Weinberg angle. It is found to be $\sin^2 \theta_W = 0.2347 \pm 0.0112$, which agree with PDG data.

A Breit-Wigner fit is performed for each decay channel. From the fit, we are able to determine total width $\Gamma_Z = (2.5370 \pm 0.0422)\,\text{GeV}$ and $M_Z = (91.1180 \pm 0.0133)\,\text{GeV}$. These values are not entirely consistent with PDG data [3]. With these two values and peak partial cross sections (generated from fit function), partial decay widths are found. Although these values have quite large uncertainties, for which the poor-quality fit should be blamed, the numbers do fit in the PDG data [3]. In the end, the invisible decay width is calculated and under assumption of validity of the Standard Model, number of neutrino generations is $N_\nu = 2.799 \pm 0.422$. It agrees again with the theory ($N_\nu = 3$).

There a few things that we assume but may introduce further uncertainties in the analysis. The number of events is assumed to be Poisson distributed thus the error is approximately $\sqrt{N}$. Reality may not strictly follow this for various reasons.

We also assumed that measured values (e.g. partial cross sections) are Gaussian distributed. All the propagation of errors is based on this fact. We have seen already that the uncertainties of peak partial cross sections are asymmetrical, meaning that they shouldn't follow Gaussian distribution. Our simplification in this step may make the error estimation onwards inaccurate.

t-channel contributions are cut out by selecting events with specific $\cos \Theta$ angles. Although the efficiencies are corrected by numerical integration, there must still be some t-channel contamination left in the events that we select as $Z^0 \to ee$ events. This could be an important reason why Breit-Wigner fit works rather poorly in ee case.

CMS energies in the actual data are not "discrete". Rather they are distributed around the seven values given in table 6. This may have some impact on the result, especially abound the resonance peak. However, a definite statement of the severity of this problem cannot be made.

A. Appendix

A.1. Raw data of several Monte Carlo samples

Event	Ctrk(N)	Ctrk(Sump)	Ecal(SumE)	Hcal(SumE)	Comment
1	2	50.9	82.6	0.0	
2	2	91.0	90.0	0.0	
3	3	82.5	92.3	0.0	
4	2	80.9	86.8	0.0	
5	2	38.1	89.5	0.0	
6	2	83.8	87.5	0.0	
7	2	87.4	93.2	0.0	
8	2	69.3	90.7	0.0	
9	2	86.1	89.4	0.5	
10	2	90.3	90.6	0.0	
11	2	92.1	88.5	0.4	
12	3	81.7	91.6	0.0	
13	2	89.6	92.5	0.0	
14	2	61.1	89.2	0.0	
15	3	88.4	89.1	0.0	
16	2	90.9	90.5	0.3	
17	2	64.6	88.8	0.0	
18	2	95.6	96.2	0.0	
19	2	93.0	90.8	0.0	
20	2	94.1	89.2	0.0	

Table 10: Measured parameter for $Z^0 \rightarrow e^+e^-$ channel

Event	Ctrk(N)	Ctrk(Sump)	Ecal(SumE)	Hcal(SumE)	Comment
1	2	90.1	1.6	7.0	
2	2	93.0	1.6	8.7	
3	2	96.8	2.0	0.0	
4	2	89.1	2.3	8.5	
5	2	90.5	1.5	7.2	
6	2	91.8	1.8	4.3	
7	2	86.3	3.7	3.3	
8	2	99.2	1.3	2.9	
9	2	88.2	1.6	3.0	
10	2	90.9	1.3	6.7	
11	2	95.6	2.5	6.1	
12	2	75.3	3.1	6.8	
13	2	85.2	5.8	4.4	
14	2	98.6	3.6	5.7	
15	2	86.8	1.9	7.9	
16	2	98.0	1.9	2.0	
17	2	108.3	2.0	8.5	
18	2	92.4	3.6	6.7	
19	2	92.0	1.9	22.6	
20	2	92.6	3.6	5.7	

Table 11: Measured parameter for $Z^0 \rightarrow \mu^+ \mu^-$ channel

Event	Ctrk(N)	Ctrk(Sump)	Ecal(SumE)	Hcal(SumE)	Comment
1	5	74.0	51.1	10.2	
2	2	46.5	17.3	8.2	
3	2	30.8	1.6	6.3	
4	2	29.5	10.2	4.1	
5	2	33.1	1.5	10.6	
6	2	24.4	12.4	11.7	
7	4	36.0	16.1	5.7	
8	2	41.3	11.1	20.0	
9	2	49.7	5.2	20.3	
10	2	33.4	23.6	6.9	
11	2	14.1	3.3	6.3	
12	2	19.7	15.9	3.8	
13	2	26.8	16.5	3.4	
14	5	23.4	27.0	17.1	
15	2	23.8	29.4	3.6	
16	2	39.0	18.9	4.4	
17	2	24.1	46.5	7.3	
18	5	38.5	28.5	0.0	
19	2	35.3	51.8	2.3	
20	2	17.8	2.5	5.0	

Table 12: Measured parameter for $Z^0 \rightarrow \tau^+\tau^-$ channel

Event	Ctrk(N)	Ctrk(Sump)	Ecal(SumE)	Hcal(SumE)	Comment
1	15	37.7	37.0	14.1	
2	17	39.2	66.8	9.9	
3	46	64.6	53.0	13.0	
5	36	45.3	53.2	7.7	
6	41	59.9	53.2	13.8	
7	9	21.9	65.2	0.0	
8	16	55.9	50.4	24.3	
9	30	38.1	68.3	13.8	
10	22	34.4	75.5	6.2	
11	36	51.2	62.3	5.5	
12	23	63.1	56.0	17.2	
13	23	59.0	60.6	8.5	
14	26	62.2	67.2	20.4	
15	30	43.3	71.7	4.3	
16	40	47.8	61.4	5.7	
17	19	67.9	52.1	10.6	
18	14	52.1	61.0	4.4	
19	29	82.6	53.8	16.4	

Table 13: Measured parameter for $Z^0 \rightarrow Hadrons$ channel

A.2. Raw data for cut efficiency

cuts	N_{ee}	$N_{\mu\mu}$	$N_{\tau\tau}$	N_{qq}
None	93 802	94 381	79 214	98 563
Pcharge and cos_thet	20 499	89 646	79 099	98 100
ee	19 817	0	651	0
$\tau\tau$	144	83 228	480	0
$\mu\mu$	314	2841	70 250	39
qq	0	0	78	92 688

Table 14: Raw data for efficiency matrix. N_i here refers to number of events in process i after some specificied cuts. Naturally ee and etc. cuts contain the Pcharged and cos_thet cuts, in particular for ee cos_thet cuts are so chosen that (almost) only s-channel events are selected.

A.3. Raw data for partial differential cross section

$\sqrt{s}$[GeV] / cuts	none	ee	$\mu\mu$	$\tau\tau$	qq
88.47	6194	125	136	157	3359
90.46	7861	198	233	207	5036
90.22	9779	223	329	249	7157
91.22	114 394	2313	3761	3247	87 844
91.97	18 931	346	664	538	14 571
92.96	8599	139	257	248	6303
93.71	10 125	191	318	281	7029

Table 15: Number of events with corresponding cms energy and cuts.

A.4. Integrated luminosity values

$\sqrt{s}$[GeV]	L	σ_L
88.47	675.9	5.7
89.46	543.6	4.8
90.22	419.8	4.0
91.22	3122.2	22.3
91.97	639.8	5.6
92.96	479.2	4.5
93.71	766.8	6.5

Table 16: Integration luminosity L for `data1.root` [2]

References

[1] Ta-Pei Cheng and Ling-Fong Li. *Gauge theory of elementary particle physics*. Clarendon Press. ISBN: 0 19 851961 3.

[2] Unknown. *Lab manual: E213 Analysis of Z0 Decay*. 2019.

[3] P.A. Zyla et al. "Review of Particle Physics". In: *PTEP* 2020.8 (2020), p. 083C01. DOI: 10.1093/ptep/ptaa104.

[4] M Lefebvre et al. "Propagation of Errors for Matrix Inversion". In: *Nucl. Instrum. Methods Phys. Res., A* 451.hep-ex/9909031 (2000), pp. 520–528. URL: https://cds.cern.ch/record/400631.

[5] Nitish Dhingra. *8.0 How to Fit a Distribution*. URL: https://twiki.cern.ch/twiki/bin/view/CMSPublic/WorkBookHowToFit.

[6] *Scipy curve fit returns negative variance*. URL: https://stackoverflow.com/questions/28702631/scipy-curve-fit-returns-negative-variance.

[7] Paolo Fornasini. *The Uncertainty in Physical Measurements*. Springer. ISBN: 978-0-387-78649-0.